Supplementary Information

Mechanistic Analysis of 5-Hydroxymethyl Furfural Electro-Oxidation via In Situ Quantification of Intermediates using Rotating Ring-Disk Electrode

Anook Nazer Eledath [a] *and Azhagumuthu Muthukrishnan* *, [a]

[a] School of Chemistry, Indian Institute of Science Education and Research

Thiruvananthapuram, Maruthamala P.O., Vithura 695551, Kerala, India

Email: muthukrishnan@iisertvm.ac.in

Calculation for finding DFF and FFCA fractions

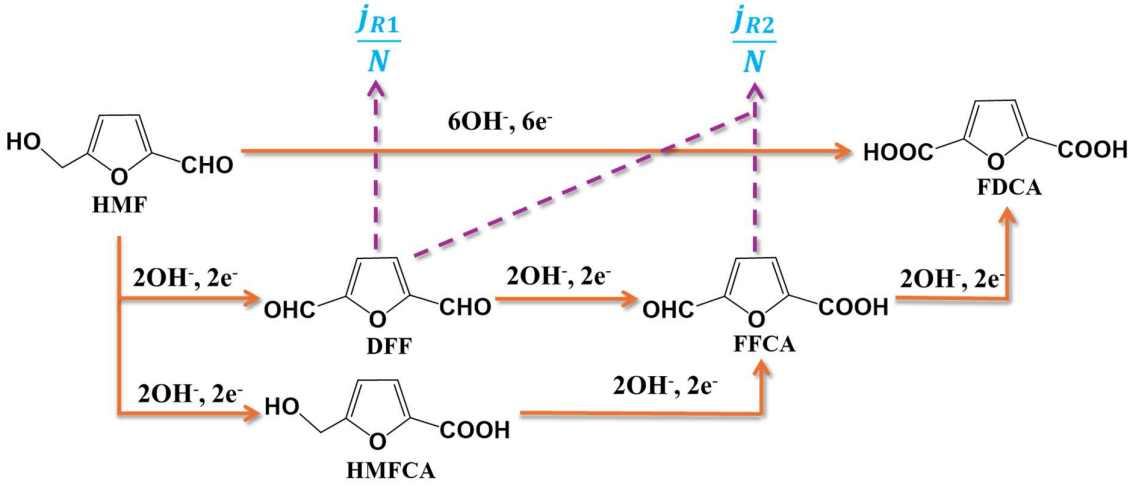

(1) Calculation of DFF Fraction (X_{DFF})

$$X_{DFF} = \frac{v_{DFF}}{v_{FDCA} + v_{FFCA} + v_{DFF}} \qquad (S1)$$

$$v_{DFF} - rate\ of\ formation\ of\ DFF$$

$$v_{FDCA} - \ rate\ of\ formation\ of\ FDCA$$

$$v_{FFCA} - \ rate\ of\ formation\ of\ FFCA$$

In general, the rate-current relationship is mentioned by ($v = j/nF$), where j, n and F refer to the current density, number of electrons and Faraday constant.

Applying this in equation S1,

$$X_{DFF} = \frac{\frac{j_{DFF}}{2F}}{\frac{j_{FDCA}}{6F} + \frac{j_{FFCA}}{4F} + \frac{j_{DFF}}{2F}} \qquad (S2)$$

Using RRDE relations

$$j_{DFF} = \frac{j_{R1}}{N} \qquad (S3)$$

Assuming the FFCA is produced via the DFF pathway

$$j_{FFCA} = \frac{2(j_{R2} - j_{R1})}{N} \quad (S4)$$

From equations (2), (3) and (4)

$$X_{DFF} = \frac{6j_{R1}}{2Nj_d + 6j_{R2}} \quad (S5)$$

(2) Calculation of FFCA Fraction (X_{FFCA})

$$X_{FFCA} = \frac{v_{FFCA}}{v_{FDCA} + v_{FFCA} + v_{DFF}}$$

Similar to the X_{DFF} derivation

$$X_{FFCA} = \frac{6(j_{R2} - j_{R1})}{2Nj_d + 6j_{R2}} \quad (S6)$$

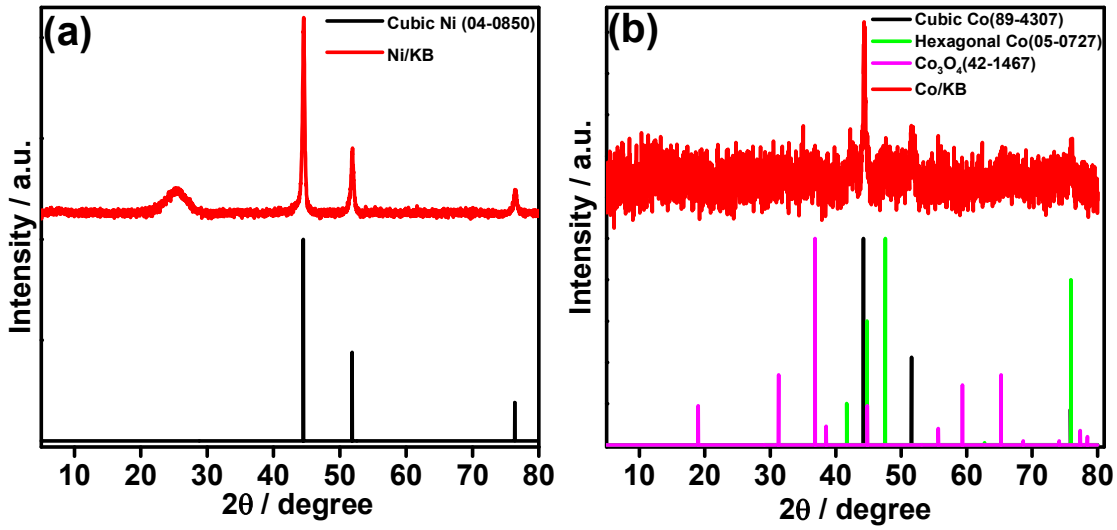

Fig. S1. Powder X-ray diffraction (PXRD) patterns of the synthesised catalysts compared with the corresponding ICDD reference data: (a) Ni/KB, (b) Co/KB.

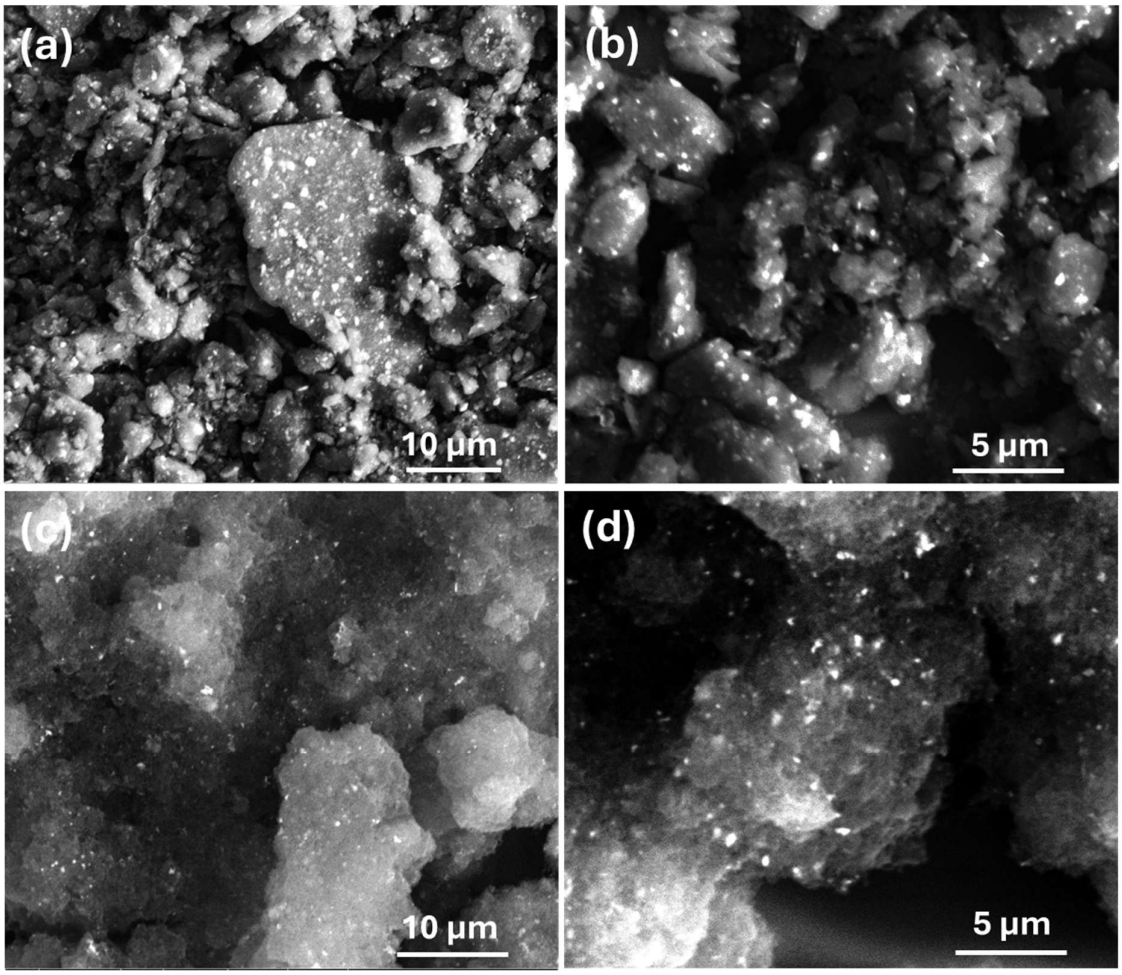

Fig. S2. SEM images of Ni/KB (a&b) and Co/KB (c&d).

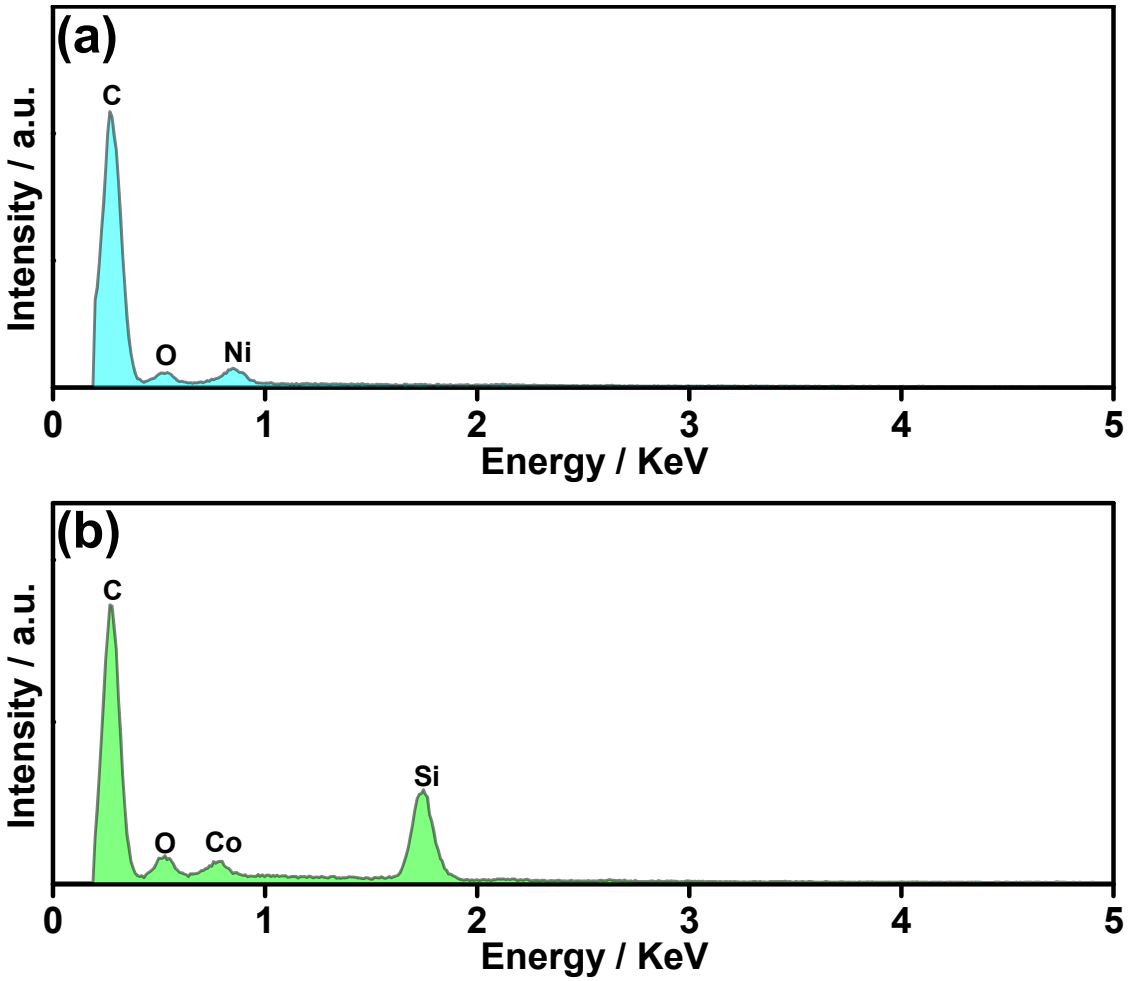

Fig. S3. EDX spectra of the synthesized Ni/KB (a) and Co/KB (b) catalysts drop-cast on a silicon wafer, confirming the presence of C, O, and the corresponding metal species; the Si signal originates from the substrate.

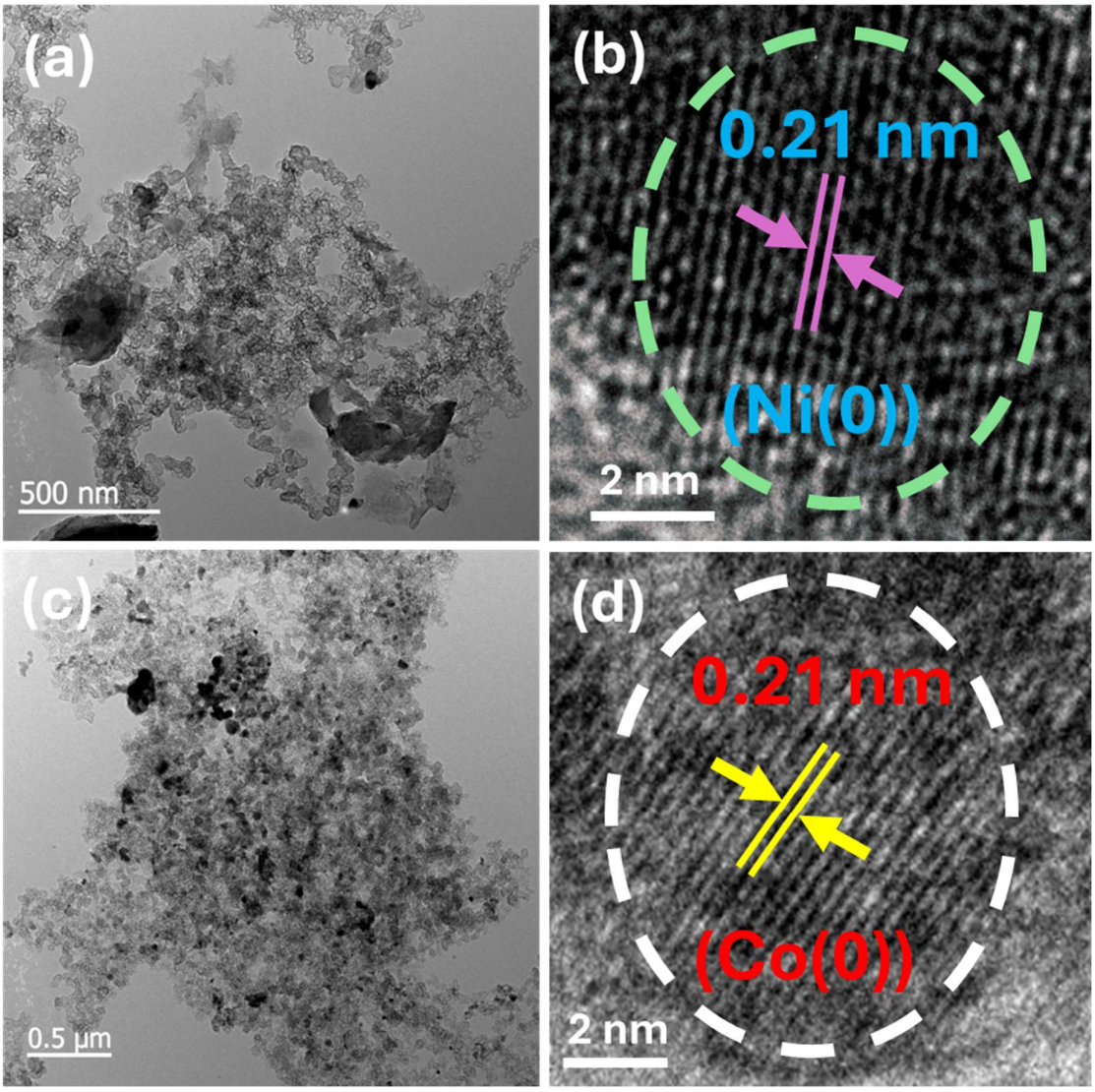

Fig. S4. TEM images of (a, b) Ni/KB and (c, d) Co/KB with the lattice fringes corresponding to metallic Ni(0) and Co(0).

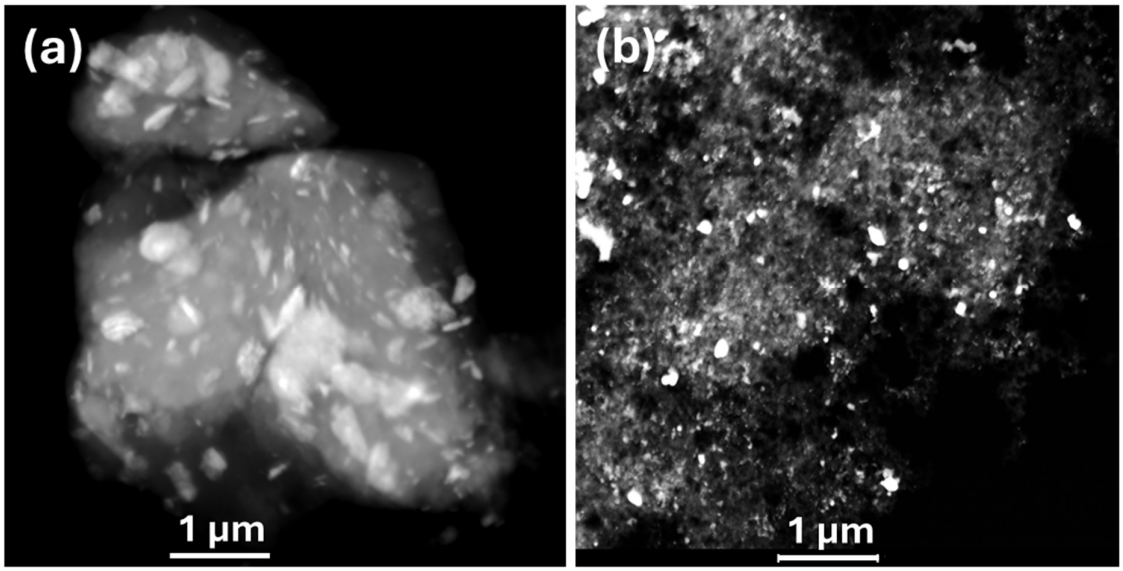

Fig. S5. HAADF-STEM images of (a) Ni/KB and (b) Co/KB.

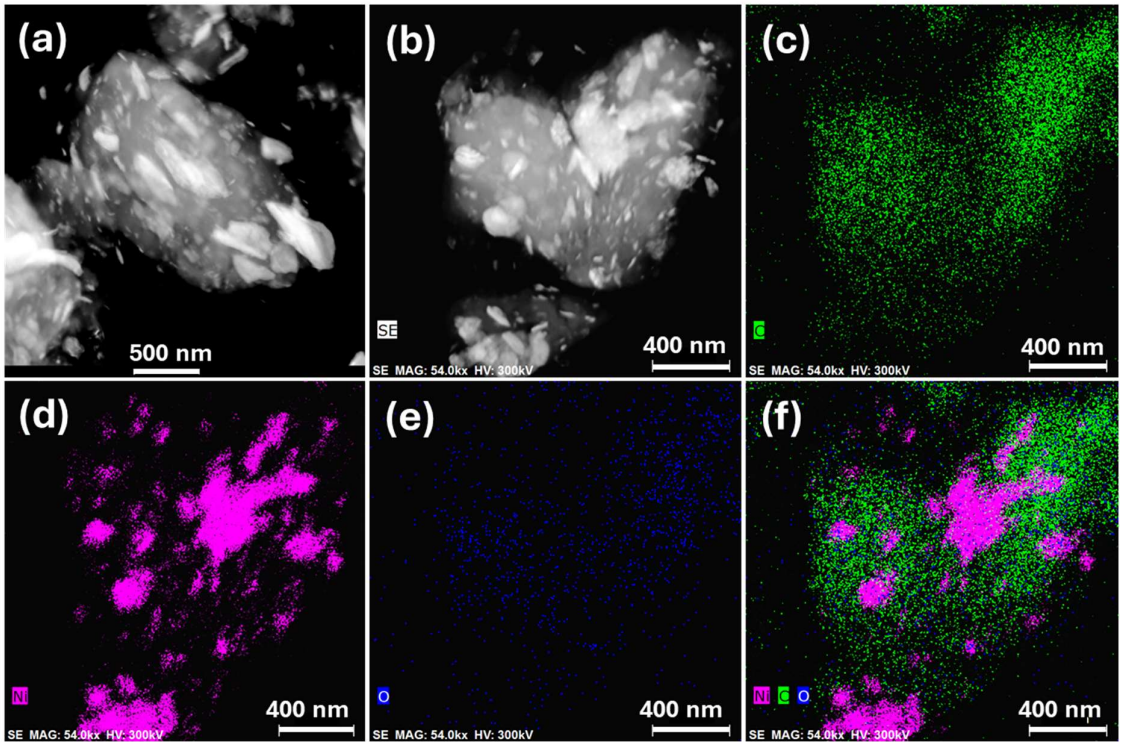

Fig. S6. (a, b) HAADF-STEM images of Ni/KB and the corresponding EDS elemental mapping of individual elements of (c) carbon, (d) nickel, (e) oxygen, and (f) all.

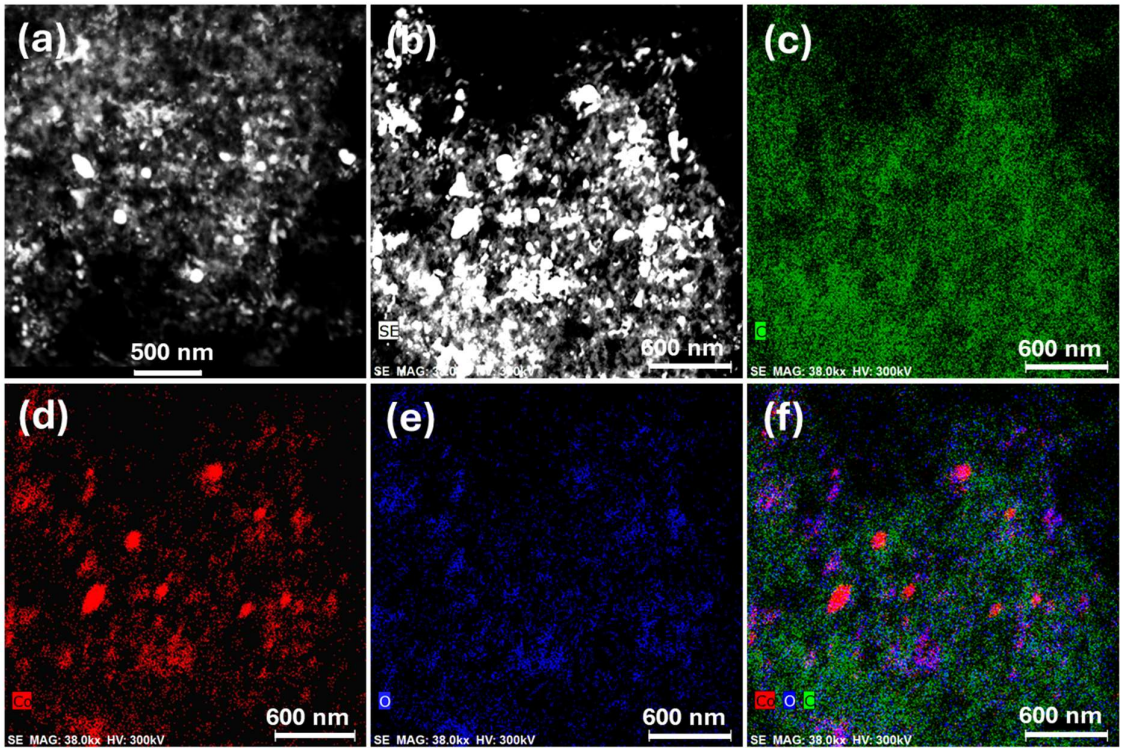

Fig. S7. (a, b) HAADF-STEM images of Co/KB and the corresponding EDS elemental mapping of individual elements of (c) carbon, (d) cobalt, (e) oxygen, and (f) all.

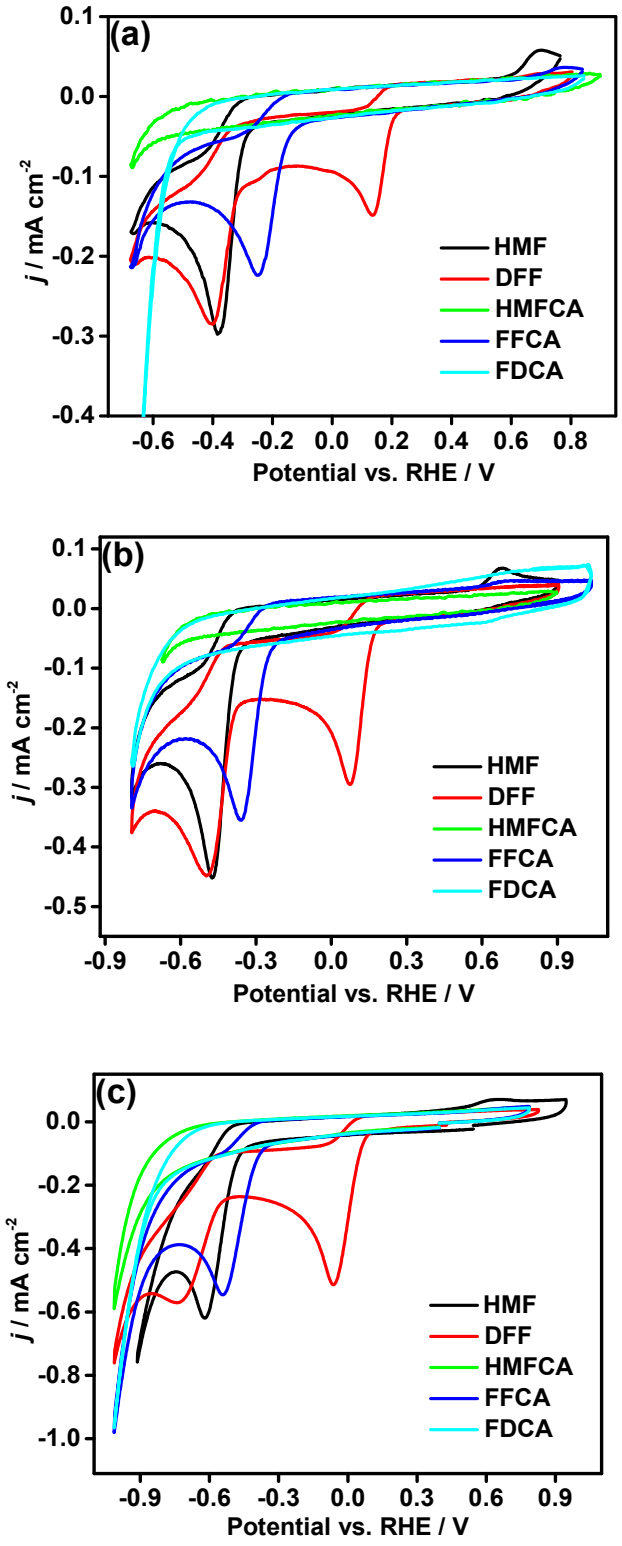

Fig. S8. Cyclic voltammograms of HMF, FDCA and its key oxidation intermediates (2 mM) recorded on a glassy carbon electrode in (a) 1 M KOH (pH 14), (b) phosphate buffer (pH 12), and (c) borate buffer (pH 10) at a scan rate of 0.1 V s^{-1}.

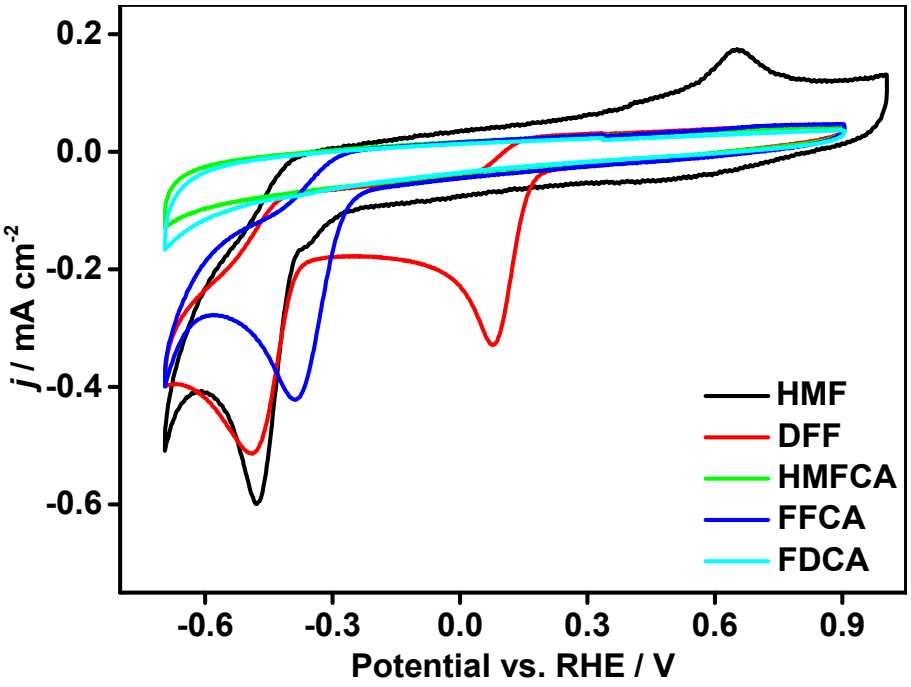

Fig. S9. Reduction potentials of FDCA, HMF and its key oxidation intermediates (2 mM) recorded on a glassy carbon electrode in 0.1 M $KClO_4$+0.1 M KOH (pH 12).

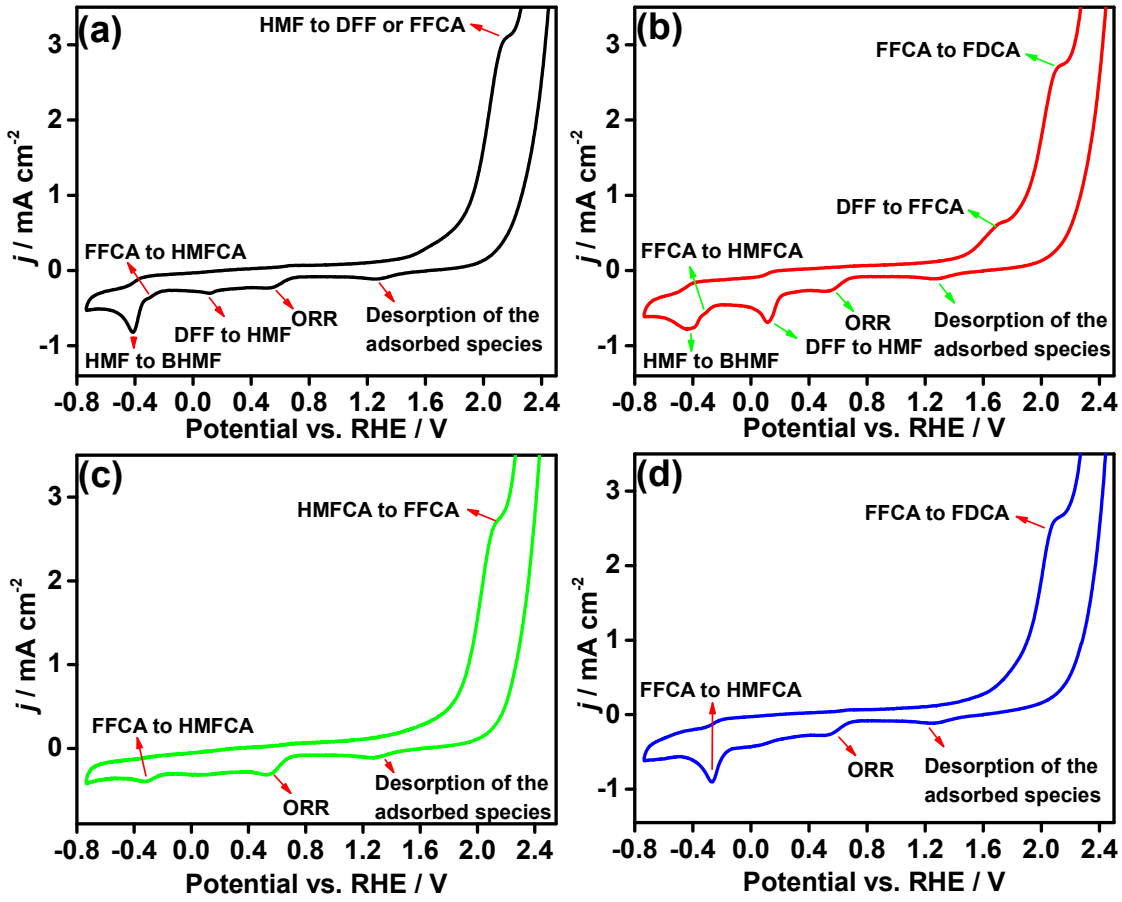

Fig. S10. Cyclic voltammograms of HMF and its key oxidation intermediates recorded at a bare GC electrode in 0.1 M KOH at a concentration of 2 mM: (a) HMF, (b) DFF, (c) HMFCA, and (d) FFCA. Measurements were carried out on a glassy carbon electrode at a scan rate of 0.1 V s^{-1}. The potential was scanned initially from the open-circuit potential toward positive potentials, then reversed to negative potentials. The characteristic oxidation and reduction features corresponding to interconversion among HMF, DFF, HMFCA, FFCA, and FDCA, as well as ORR and desorption of adsorbed species, are indicated.

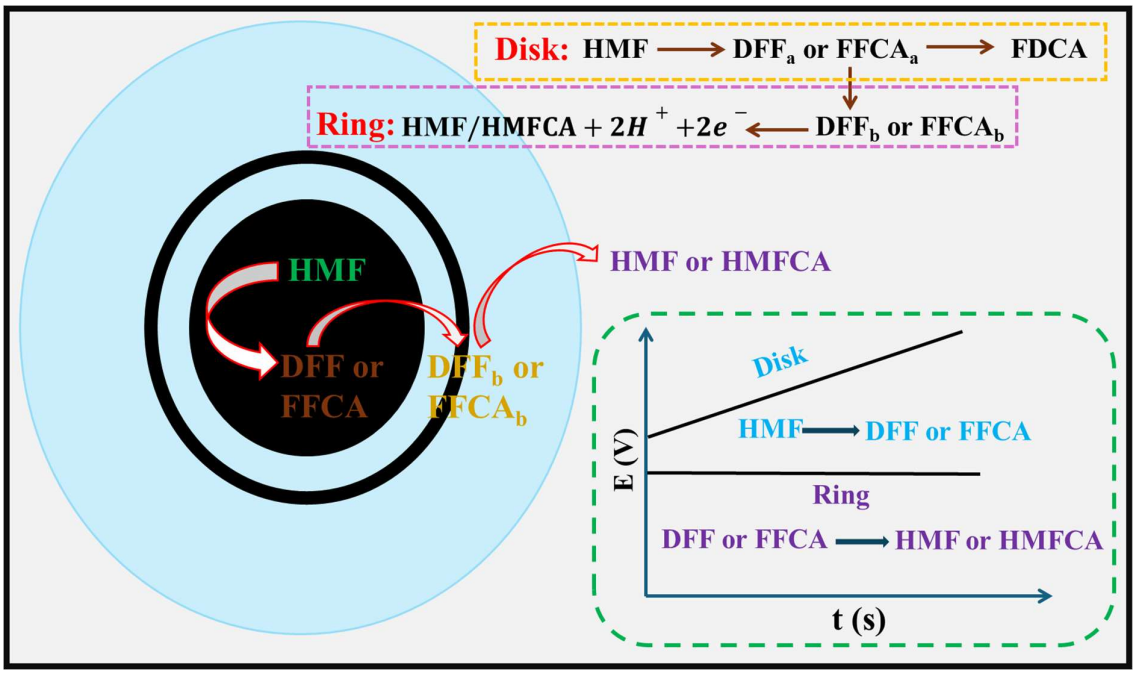

Fig. S11. Schematic of in situ RRDE measurements for HMF oxidation, where HMF is oxidized at the disk via DFF or HMFCA pathways. The resulting intermediates are moved to the ring and selectively reduced for real-time detection; DFF is directly quantified, while the HMFCA pathway is indirectly monitored via FFCA reduction.

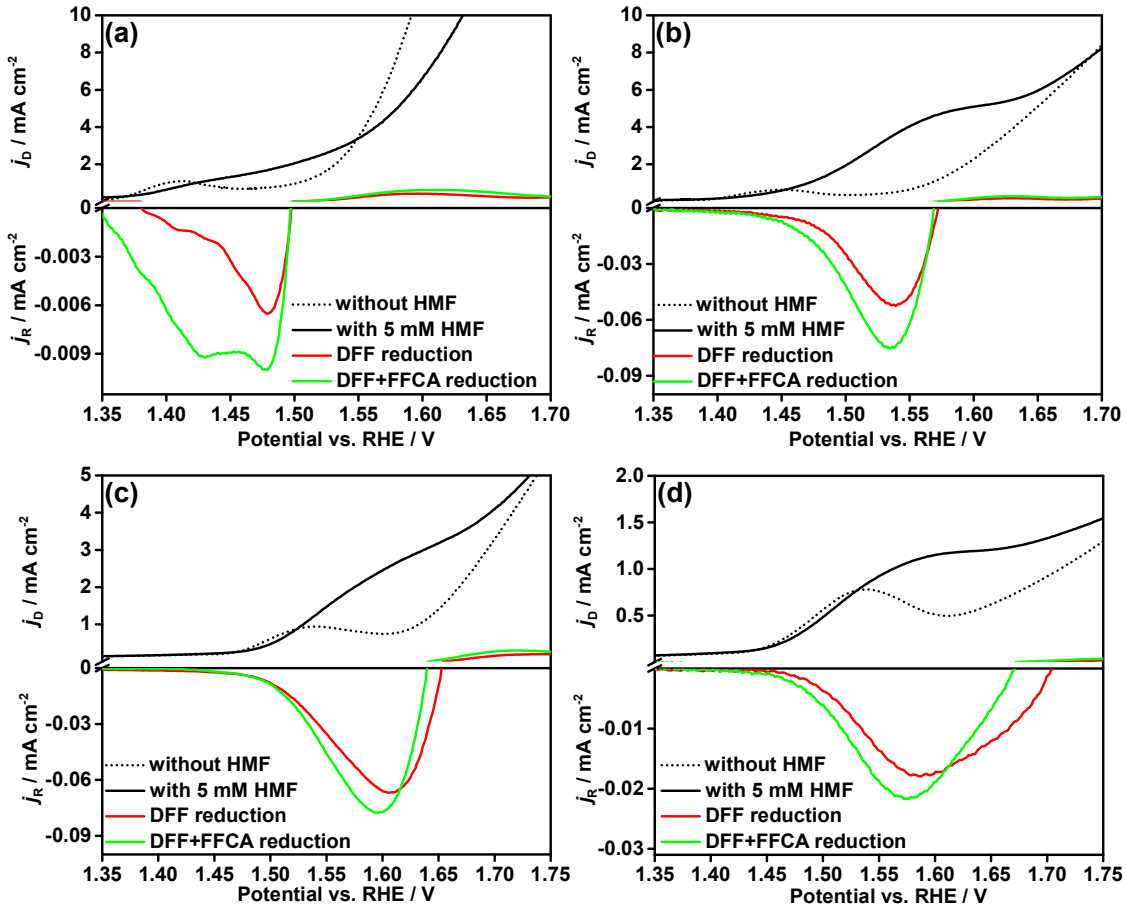

Fig. S12. RRDE voltammograms of Ni/KB coated on a glassy carbon electrode for probing reaction intermediates during HMF oxidation. The disk potential was scanned anodically at 2 mV s^{-1}, while the ring was maintained at a fixed potential to selectively detect the reduction of DFF and FFCA. Measurements were performed in (a) 1 M KOH (pH 14), (b) 0.1 M KOH (pH 13), (c) phosphate buffer (pH 12), and (d) borate buffer (pH 10). Ring currents were background-subtracted to isolate intermediate-related signals.

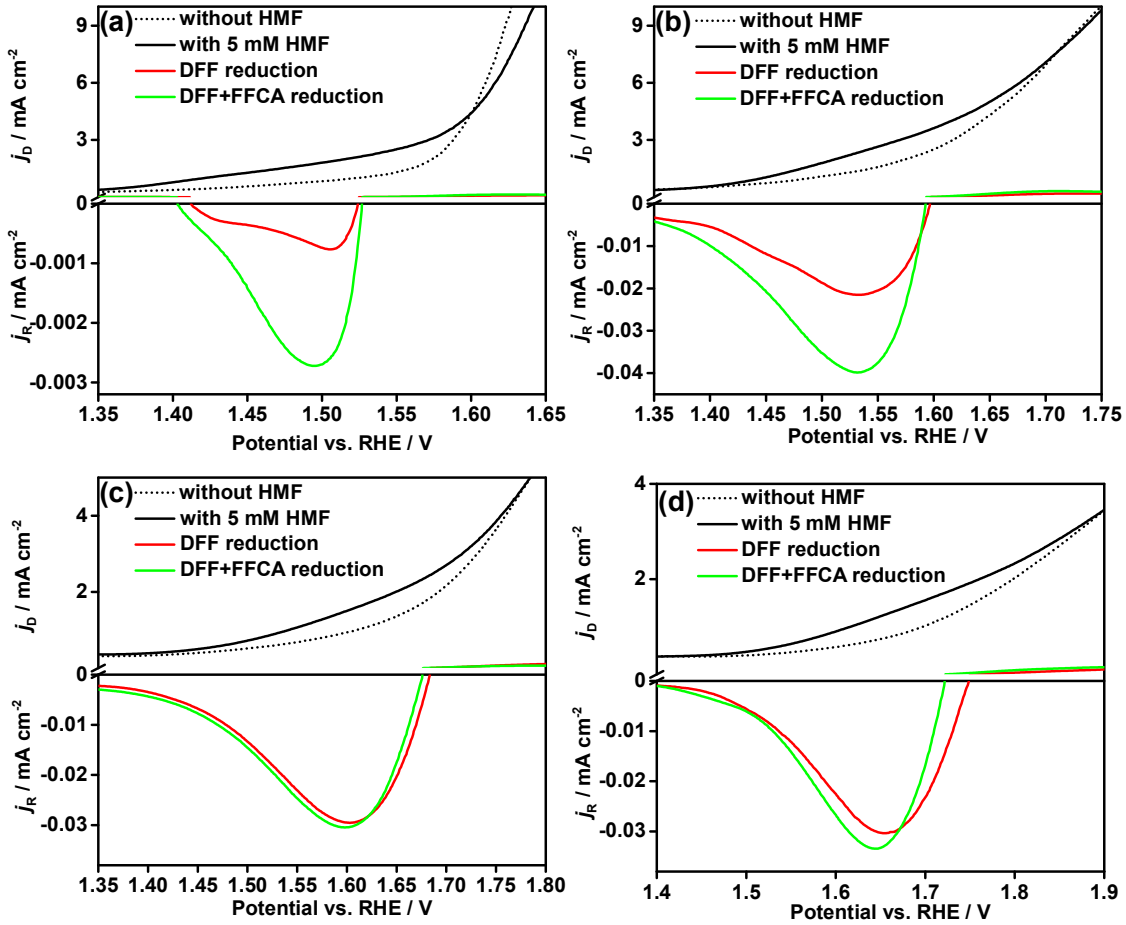

Fig. S13. RRDE voltammograms of Co/KB coated on a glassy carbon electrode for probing reaction intermediates during HMF oxidation. The disk potential was scanned anodically at 2 mV s^{-1}, while the ring was maintained at a fixed potential to selectively detect the reduction of DFF and FFCA. Measurements were performed in (a) 1 M KOH (pH 14), (b) 0.1 M KOH (pH 13), (c) phosphate buffer (pH 12), and (d) borate buffer (pH 10). Ring currents were background-subtracted to isolate intermediate-related signals.

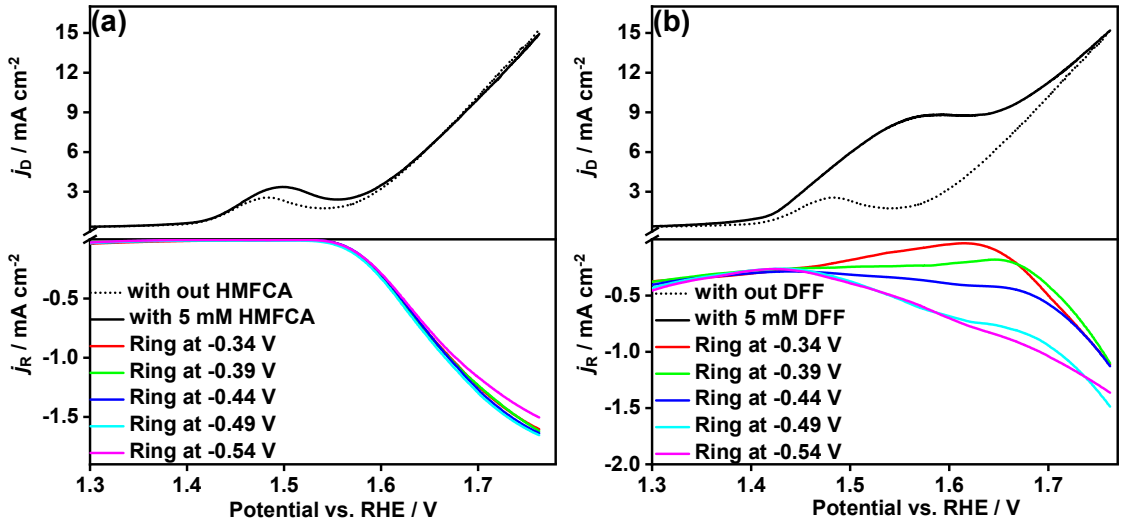

Fig. S14. Rotating ring-disk electrode (RRDE) voltammograms were recorded in 0.1 M KOH at a scan rate of 5 mV s^{-1}, with Ni/KB coated on the disk electrode. (a) Disk and ring current responses in the absence and presence of 5 mM HMFCA. (b) Disk and ring current responses in the absence and presence of 5 mM DFF. Ring currents were collected at different ring potentials (-0.34 to -0.54 V), highlighting the formation and detection of reaction intermediates during electrochemical oxidation.

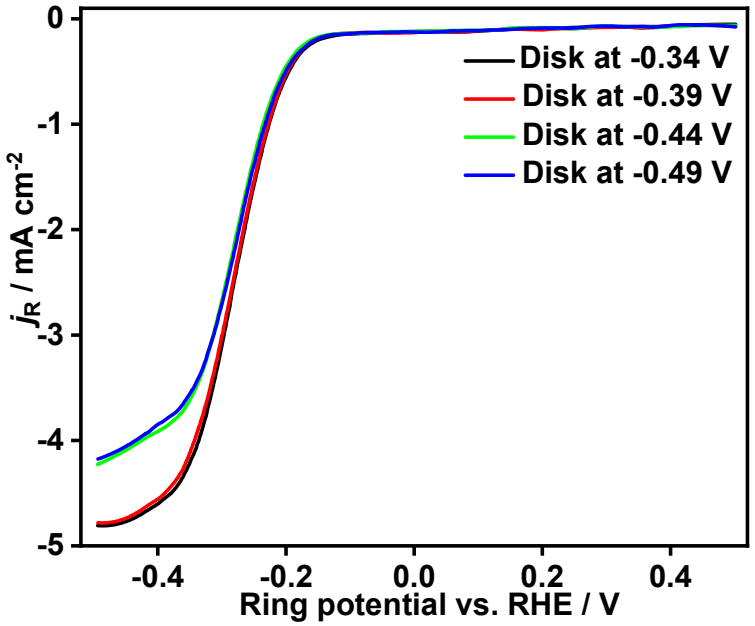

Fig. S15. Ring current responses recorded in 0.1 M KOH with 5 mM FFCA during RRDE measurements, where the disk GC electrode was held under chronoamperometric conditions at selected potentials (-0.34, -0.39, -0.44, and -0.49 V vs. RHE) corresponding to FFCA reduction. The ring potential was swept cathodically at a scan rate of 10 mV s^{-1} to probe the reduction of soluble intermediates generated during FFCA reduction at the disk.